α-transfer contribution to $^{10}B+^{14}N$ elastic scattering

H. Takai* and K. Koide
Instituto de Fisica, Universidade de São Paulo, São Paulo, Brazil

A. Bairrio Nuevo, Jr.
Instituto de Fisica, Universidade Federal do Rio de Janeiro, Rio de Janeiro, Brazil

O. Dietzsch
Instituto de Fisica, Universidade de São Paulo, São Paulo, Brazil
(Received 18 April 1988)

Elastic scattering $^{10}B(^{14}N,^{14}N)^{10}B$ angular distributions were measured at four bombarding energies: 38.1, 42.0, 46.0, and 50.0 MeV. By detecting the recoiling target nuclei complete angular distributions ranging from $\theta_{c.m.}=14°$ to 176° were obtained. Normalized cross sections, σ/σ_R were found to be larger than 0.1 for angles greater than 160°. The anomalous behavior at the backward angles is interpreted as partially due to an elastic α-transfer process. The deduced spectroscopic factor for the configuration of an alpha particle coupled to a ^{10}B core in the ^{14}N ground state is $S_4=0.65\pm0.10$. The compound elastic contribution is about 20% of the calculated transfer cross section at $\theta=176°$ and accounts for 3% of the experimental cross section at this angle.

I. INTRODUCTION

Enhancement of the elastic scattering cross section at backward angles has previously been observed in systems where both projectile and target nuclei belong to the $1p$ and/or s-d shells.[1-5] This effect has been found to be more pronounced when the mass difference between target and projectile is small (one or two nucleons) or when both nuclei are an integer multiple of an alpha particle, e.g., ^{12}C or ^{16}O. Pronounced structures in both angular distribution and excitation functions, for example, have been measured in systems such as $^{16}O+^{28}Si$ (Ref. 1) and $^{16}O+^{17}O$ (Ref. 2). Traditional optical model calculations have failed to reproduce the experimental data unless unphysical optical model parameters are introduced, but in several cases,[2,3] the observed structures in the cross section curves could be reproduced by the inclusion of single nucleon or cluster transfer amplitudes in the total scattering amplitude.

Exchange of nucleons or alpha particles between the scattering partners has been found to play a major role in many cases, especially if two $n\alpha$-type nuclei are present. The back-angle elastic cross section for $^{16}O+^{17}O$ and $^{16}O+^{12}C$, for instance, has been attributed to a neutron[2] and an alpha-particle[3] exchange, respectively. In general, the observation of backward angle elastic cross section enhancement is favored for $1p$-shell systems if the projectile and target nuclei exhibit large spectroscopic amplitudes for cluster or single nucleon configurations. However, such enhancement is also observed in other cases such as $^{12}C+^{19}F$ (Ref. 4) and $^{10}B+^{16}O$ (Ref. 6), where the mass asymmetry is larger than an α particle. In these cases mechanisms different from nucleon or cluster exchange could be involved.

To investigate the presence of such phenomena for non-$n\alpha$ nuclei and mass differences larger than one or two nucleons, the elastic scattering of ^{14}N by ^{10}B was studied. Neither nucleus has an $n\alpha$ structure, although it is known that the spectroscopic amplitude for ^{14}N in its ground state, described as a core of ^{10}B coupled to an α particle, is quite large. Alpha-transfer experiments[7,8] and theoretical results[9] have shown a spectroscopic amplitude for the ^{14}N ground state comparable to most $n\alpha$ nuclei in the $1p$ shell, e.g., $^{12}C+\alpha$. The excitation function for the elastic scattering at $\theta_{c.m.}=172°$ for the $^{10}B+^{14}N$ reaction has been previously investigated by Marquardt and collaborators.[10] The results derived from their study show the presence of broad structures as compared to other cases such as $^{16}O+^{28}Si$. Furthermore, resonancelike structures have been observed in the excitation functions of the $^{10}B(^{14}N,^{12}C)^{12}C$ and $^{12}C(^{12}C,^{10}B)^{14}N$ reactions.[11,12] These resonances were tentatively assigned as being molecular rotational states of ^{24}Mg formed in an intermediate step of the reaction.

The bombarding energies chosen for the present experiment were based on the results of the above-mentioned reactions. The lower two, 38.1 and 42.0 MeV, were chosen to be on the excitation function structure tentatively associated[12] with a $J^\pi=16^+$ state in ^{24}Mg. The other two bombarding energies, 46.0 and 50.0 MeV, were chosen to be out of any other "resonance" peak.

In Sec. II we present the experimental techniques employed to obtain a complete angular distribution from $\theta_{c.m.}=16°$ up to $\theta_{c.m.}=176°$. In Sec. III we describe the analysis of the experimental data. The discussion of our results and some of the conclusions obtained are presented in Sec. IV.

II. EXPERIMENTAL METHODS

Beams of ^{14}N ions produced by the electrostatic accelerator at the University of Sao Paulo were used to

bombard thin self-supported ^{10}B ($\simeq 50$ $\mu g/cm^2$) targets. The targets were surrounded by a cryogenic trap (77 K) and the vacuum in the scattering chamber was kept around 1×10^{-6} Torr in order to avoid significant carbon buildup.

In order to determine a complete angular distribution from $\theta_{c.m.}=16°$ up to $\theta_{c.m.}=176°$, two different experimental arrangements were used. In both cases, the cross sections at backward angles ($\theta_{c.m.}>100°$) were determined by detecting the recoiling target nuclei at forward angles. To detect the reaction products corresponding to intermediate angles, $60°<\theta_{c.m.}<120°$, a 60 cm diameter scattering chamber was used. A ΔE(18 μm)-E(100 μm) silicon telescope, mounted in the chamber, allowed the detection and identification of ions of ^{14}N, elastically scattered from the target, as well as the recoiling ^{10}B nuclei and other reaction products.

For the detection of particles at forward angles ($\theta_{lab}<25°$) an Enge split-pole magnetic spectrograph was employed. Two different gas-filled position-sensitive detectors were used to detect the particles in the focal plane of the instrument. The first detector,[13] a drift chamber with a delay line readout, was employed to obtain the data for $E_{lab}=38.1$ and 42.0 MeV bombarding energies. The second detector,[14] a hybrid E-ΔE position-sensitive detector, with a delay line readout, became available later and was mainly used to extract data for $E_{lab}=46.0$ and 50 MeV bombarding energies.

The magnetic spectrograph setup could be used to detect the elastic scattered particles down to $\theta_{lab}=7°$ due to the instrument resolving power. The magnetic spectrograph was also employed to detect the recoiling target nuclei. In this case, the detectors were covered with aluminum absorbers of thicknesses chosen so as to avoid the intense elastic flux and to allow for the detection of recoiling ^{10}B ions at forward angles. Typical experimental spectra obtained with the magnetic spectrograph are shown in Figs. 1(a) and 1(b) for ^{14}N and ^{10}B detected at forward angles, respectively. The spectrum in Fig. 1(a) shows, among other characteristics, a low yield for ions scattered from both ^{11}B and ^{12}C contaminants. The position resolution for ions scattered off ^{10}B is typically 2.5 mm which corresponds to an energy resolution of approximately 140 keV. Such resolution allowed for a clear identification of the several peaks in the spectrum. Similarly, the recoil spectrum in Fig. 1(b) shows a clear separation between different reaction products. The energy resolution for recoiling ions is about 250 keV, mostly due to multiple scattering in the aluminum absorber. Carbon groups from the reaction $^{10}B(^{14}N,^{12}C)^{12}C$ are indicated in the spectrum of Fig. 1(b).

In both experimental setups two silicon detectors symmetrically placed at fixed angles with respect to the beam direction allowed the normalization of the cross sections and the monitoring of the beam direction. A Faraday cup was also used to integrate the total incident current on target. The data at each angle were normalized with respect to the monitor counts, and quantities proportional to σ/σ_R were derived. Proper solid angle corrections were applied to the data obtained by detecting ^{10}B ions in recoil. The experimental points obtained with the magnetic spectrograph were also corrected for the ion charge state by using experimental charge distributions measured at frequent intervals during the data taking periods. The data from different experimental setups were normalized with respect to each other at a minimum of five different angles. The quantities propor-

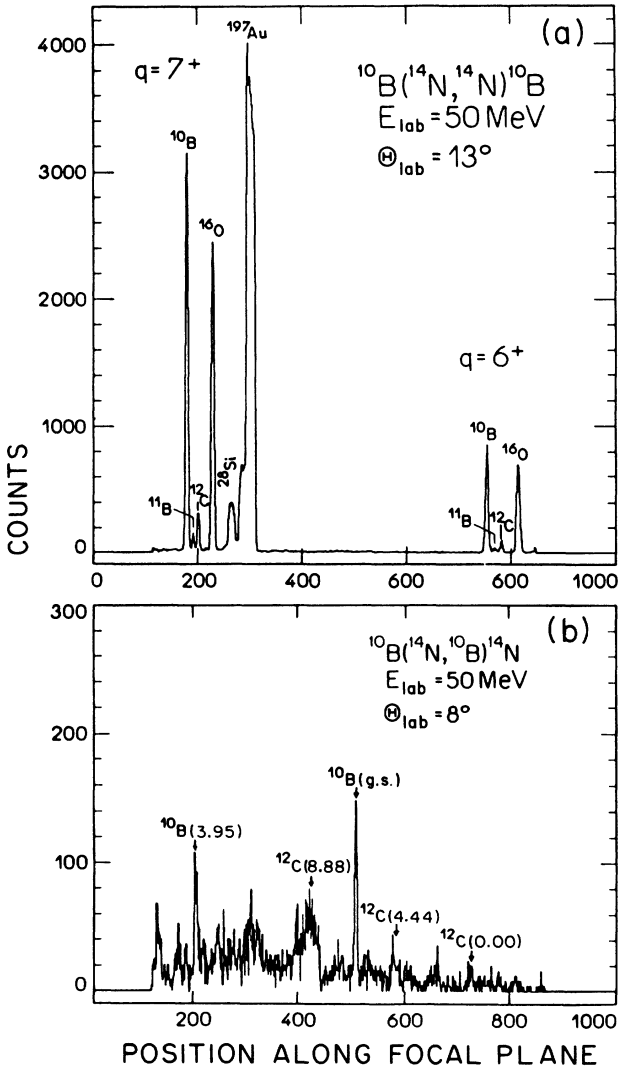

FIG. 1. (a) Spectrum of ^{14}N ions scattered by a ^{10}B target as observed in a position-sensitive detector at the focal plane of an Enge split-pole magnetic spectrograph. Two ^{14}N charge states, $q=7$ and 6, are present. Ions scattered from contaminants are also seen. Resolution for the peak labeled ^{10}B is approximately 140 keV. The group labeled ^{197}Au corresponds to scattering from a thin gold layer in the target and is considerably broadened due to being focused at a focal plane different from the light target nuclei. The ^{197}Au peak for the charge state 6^+ falls out of the limits of the detection system. (b) Typical spectrum for the recoil of ^{10}B at forward angles. The peak corresponding to the recoiling target nuclei in its ground state is indicated. A peak that corresponds to the projectile excitation (3.95 MeV) is also indicated. The energy resolution for the ^{10}B peaks is typically 250 keV. The carbon peaks originate from the reaction $^{10}B(^{14}N,^{12}C)^{12}C$.

TABLE I. Optical model parameters from fits to elastic scattering excitation functions at $\theta_{c.m.}=48.6°$ and 74.4°. The parameters are from Ref. 11.

V_R (MeV)	r_R[a] (fm)	a (fm)	W_0[b] (MeV)	W_1 (MeV)	r_I[a] (fm)	a_I (fm)	R_C (fm)
28.85	1.29	0.56	13.13	0.74	1.34	0.30	6.16
14.41	1.39	0.54	17.80	0.63	1.34	0.32	6.36

[a]The radii are calculated as $R_{R,I}=r_{R,I}(A_T^{1/3}+A_P^{1/3})$, where A_P and A_T are the projectile and target mass numbers, respectively.
[b]The depth of the imaginary potential is calculated by $W_I=W_0+W_1E_{c.m.}$.

tional to σ/σ_R were then normalized at forward angles ($\theta_{c.m.}<60°$) to optical model predictions, using the energy-dependent parameters of Hoppe and collaborators[11] listed in Table I. The overall uncertainty associated with each experimental point varies from 10% to 17%, depending on the number of counts in the elastic peak at each angle.

III. RESULTS AND DATA ANALYSIS

A. Results

The experimental angular distributions for the four bombarding energies are shown in Fig. 2. The overall shape of the angular distributions resembles the behavior observed for other systems[1-5] that exhibit back-angle cross section enhancement. The angular period of the strong oscillating structure at forward angles decreases as the bombarding energy is increased. As suggested by the diffraction model,[15] the angular period ($\Delta\theta$) of oscillation is related to the grazing angular momentum l_g for the scattering by $\Delta\theta=\pi/l_g$. The structures present at intermediate angles are characteristic of each bombarding energy, and although an interferencelike pattern is observed, these structures are not as pronounced as in other $1p$ systems.[2,5] At larger angles, a rise in the cross section for all energies is observed with $\sigma/\sigma_R>0.1$ for $\theta>160°$. The structure present in this region also exhibits a dependence on bombarding energy. The oscillations, however, are characterized by a larger angular period, thus suggesting a reaction mechanism originating from partial waves with $l<l_g$ in the collision.

In the angular region between 140° and 160°, a local maximum is present in all angular distributions. The position of this maximum moves towards larger angles as the bombarding energy is increased, but the overall shape and intensity of the angular distribution at these backward angles for the four bombarding energies are very similar. This is consistent with the observation that the strong resonancelike structures seen in the excitation function[12] of the reaction $^{10}B(^{14}N,^{12}C)^{12}C$ do not manifest strongly in the elastic channel[10] at backward angles.

The very forward parts of the angular distributions, $\theta<60°$, are well fitted by the optical model cross sections using the energy-dependent parameters of Hoppe and collaborators.[11] These parameters, listed in Table I, were obtained from fits to excitation functions for the elastic scattering at $\theta_{c.m.}=48.6°$ and $\theta_{c.m.}=74.4°$. The use of

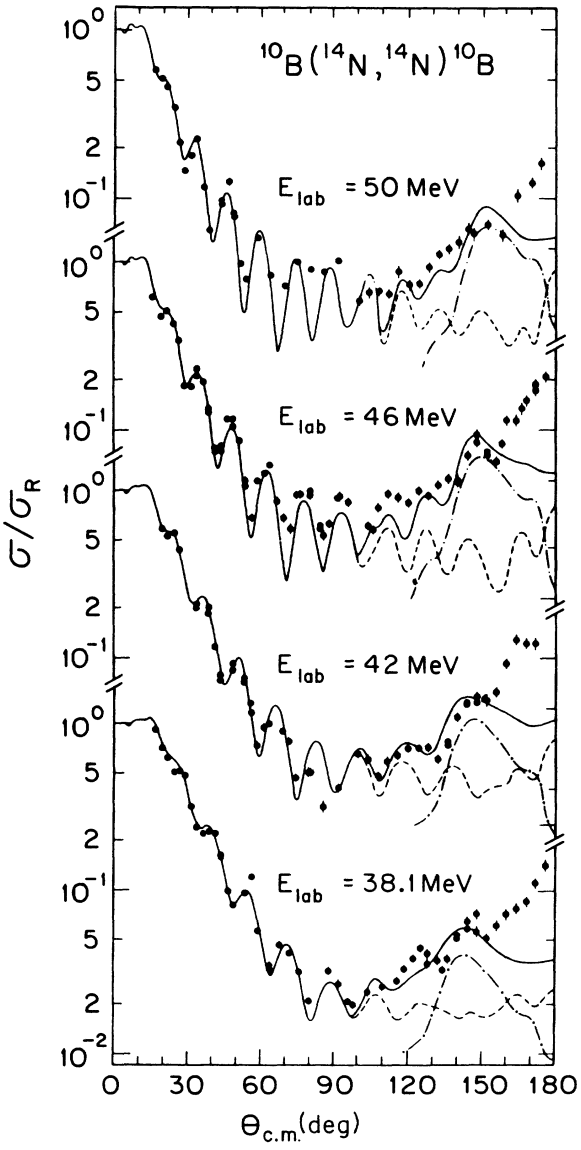

FIG. 2. Experimental angular distributions for the elastic scattering of ^{14}N by ^{10}B at four bombarding energies. The error bars indicated in the figures correspond to statistical errors only. The solid lines are the results of the elastic-transfer calculations. The dashed lines at backward angles represent the cross sections resulting from the coherent addition of the elastic scattering amplitude with the $l=0$ alpha transfer amplitude. The dot-dashed lines represent the incoherent sum of transfer amplitudes for $l>0$.

any of the parameters in Table I results in similar curves with weakly attenuated angular distributions at backward angles. The optical model cross sections are typically 10% of the experimental data at $\theta_{\text{c.m.}}=176°$. In order to understand the nature of the elastic cross section at backward and intermediate angles, the contribution of two possible competing reaction processes, namely the elastic-transfer process and the compound-elastic process, were evaluated

B. Elastic transfer

The large spectroscopic amplitude[9] for the configuration of ^{14}N as an α particle coupled to a ^{10}B core suggests that the elastic-transfer process may be a strong component in the total elastic scattering cross sections. The exchange of an α particle between target and projectile should be favored, since the ground state of ^{14}N exhibits a larger cluster component than excited levels.[9] Taking the elastic-transfer process into account, the total elastic cross section can be written as follows:

$$\frac{d\sigma}{d\Omega}=[T_{\text{el}}\pm T_{\text{tr}}^{l=0}(\pi-\theta)]^2+\sum_{l>0}[T_{\text{tr}}^{l>0}(\pi-\theta)]^2 , \quad (1)$$

where T_{el} and T_{tr} are the elastic and the alpha-particle transfer amplitudes, respectively. This expression contains two distinct terms: (a) a term with the elastic scattering amplitude and the $l=0$ amplitude for alpha transfer interfering coherently and (b) the incoherent contribution of all other l transfers. The angles for the transfer amplitudes are reversed by π. Both positive and negative signs for the transfer amplitude in the first term of the equation were considered in the calculations. The elastic scattering amplitudes were evaluated within the finite range DWBA approximation. Recoil effects were also taken into account in the calculations. As the ground state spin-parity of ^{14}N is $J^{\pi}=1^{+}$, an alpha particle coupled to a ^{10}B core with $J^{\pi}=3^{+}$ can be found in two differential orbitals with angular momentum $L=4$ or $L=2$. The configuration with the higher angular momentum should be favored since it locates the cluster in a more peripheral orbit with a larger average radius. The theoretical spectroscopic factors as derived by Kurath[9] are $S_4=0.70$ and $S_2=0.01$, respectively, for the two above-mentioned configurations. In the calculations, the α cluster quantum numbers for a given configuration were obtained from the harmonic oscillator approximation:[16]

$$\sum 2n_i+l_i=2N+L=4 , . \quad (2)$$

where n_i and l_i are the quantum numbers for the cluster constituent nucleons in ^{14}N, and N and L are the principal and orbital quantum numbers for the cluster which is coupled to the ^{10}B core. The transferred angular momentum l_{tr} can range from $l=0$ to $l=8$ when an $L=4$ orbital is assumed for the α cluster in the projectile and residual nuclei. Similarly, l_{tr} can assume any value from $l=0$ to 4 when $L=2$ is assumed. When mixed configurations are considered, angular momentum transfers from $l=0$ to 6 need to be taken into account. The cluster wave functions were generated in the present calculation by adjusting the depth of a Woods-Saxon well in order to reproduce the α-particle binding energy of 11.6 MeV in ^{14}N.

To evaluate contributions from the elastic and the $l=0$ transfer, the scattering amplitudes were generated by the exact finite range (EFR) DWBA code LOLA.[17] The DWBA amplitudes weighted with a spectroscopic factor were then coherently added to elastic amplitudes, angle by angle, as indicated in expression (1). Due to the time consuming numerical integration algorithm used by the code LOLA, this program was found to be inappropriate for calculations where high angular momentum transfer is involved. The contributions from $l>0$ were then calculated using the EFR-DWBA code SATURN–MARS.[18] Before obtaining the cross sections for the incoherent sum the results of the two codes were checked up to $l=4$ transfers with the same input parameters. An agreement within 10% in the cross section calculated by the two programs was found. Since the cluster configuration with $L=4$ has a theoretical spectroscopic factor much larger than the one with $L=2$, only the former was taken in consideration. The transfer cross sections for which an $L=2$ orbital is involved were evaluated for $E=46$ MeV and they have been verified to be of the order of 3% of the experimental elastic transfer cross section at $\theta_{\text{c.m.}}=176°$. For the evaluation of the incoherent sum transfer amplitudes, T_{tr} for l_{tr} as large as 8 were generated.

The results of the calculations for the four bombarding energies are shown in Fig. 2 together with the experimental angular distributions. In this figure, the coherent and incoherent sums are shown separately. The same spectroscopic factor of $S_4=0.65$ was used for all energies. This value gave the best fit to the experimental data for all bombarding energies. An uncertainty in S_4 of ± 0.10 accounts for a range of variation in the spectroscopic factor values for which satisfactory fits are still verified. Due to the presence of high-valued angular momentum transfers, the incoherent sum in Eq. (1) is the predominant contribution to the elastic transfer cross section. In all calculations, positive and negative signs for the coherent sum in Eq. (1) were allowed, but since large angular momentum transfer dominates the angular distributions at backward angles, no appreciable effect was observed. The α-particle transfer process results in a "bell-shaped" curve that quite satisfactorily reproduces both the shape and intensity of the experimental structure present around $\theta_{\text{c.m.}}=150°$ in the four angular distributions. In particular, the angular position dependence with the energy is well described, thus suggesting that the elastic-transfer process is responsible for the origin of this structure.

The addition of the α elastic-transfer amplitude to the optical potential scattering amplitudes reproduces the experimental cross sections quite well up to 160°, describing the approximate shape and intensity of the experimental data. However, the elastic-transfer process fails to reproduce the sharp rise in the experimental data at the very backward angles (160°–180°).

TABLE II. Optical model parameters for statistical model calculations.

Channel	V (MeV)	R (fm)	a (fm)	W (MeV)	R_I (fm)	a_I (fm)	R_C (fm)
$^{10}B+^{14}N$[a]	14.4	6.35	0.54	$17.8+0.63E_{c.m.}$	6.10	0.32	6.36
$^{12}C+^{12}C$[b]	14.0	6.18	0.35	$0.40+0.10E_{c.m.}$	6.41	0.56	6.18
$^{8}C+^{16}O$[c]	14.0	6.10	0.49	$0.40+0.15E_{c.m.}$	6.41	0.49	6.10
$\alpha+^{20}Ne$[c]	50.0	4.94	0.59	2.00	4.94	0.46	4.94
$p+^{23}Na$[c]	$56.0-0.55E_{c.m.}$	3.56	0.65	13.50	3.56	0.47	3.56
$n+^{23}Mg$[c]	$48.2-0.30E_{c.m.}$	3.56	0.65	11.50	3.56	0.47	0.00
$d+^{22}Na$[d]	$88.9-0.33E_{c.m.}$	3.72	0.81	$14.4+0.24E_{c.m.}$	3.57	0.68	3.32

[a]Reference 11.
[b]Reference 26.
[c]Reference 27.
[d]Reference 28.

C. Compound-elastic channel

In order to investigate a possible contribution to the backward angle cross section from the compound-elastic channel, a statistical model calculation was performed. The calculations were done within the Hauser-Feshbach formulation using the code STAT−2.[19] As listed in Table II, a total of nine compound nucleus decay channels were considered, including the elastic channel. The ^{12}C(4.44 MeV) + ^{12}C and ^{8}Be(2.94 MeV) + ^{16}O channels were also included, since they are strongly populated in the $^{10}B(^{14}N,^{12}C)^{12}C$ and $^{10}B(^{14}N,^{8}Be)^{16}O$ reactions as observed by Marquardt and collaborators.[10] Table II lists the optical model parameters for the respective channels. The level density and pairing energy parameters are listed in Table III. The level density and pairing parameters for the compound nucleus, ^{24}Mg, used in the calculations are $a=3.58$ MeV^{-1} and $\Delta=5.13$ MeV, respectively. These parameters were taken from the study[11] of the reaction $^{10}B(^{14}N,\alpha)^{20}Ne$. Discrete energy levels for all channels were used in the calculations to minimize the dependence of the level density parameters on the results. With no restrictions on the angular momentum of the compound nucleus, the compound-elastic channel was verified to contribute as much as 50% of the elastic-transfer process at $\theta_{c.m.}=180°$. However, neither shape nor intensity of the backward angle angular distribution was reproduced satisfactorily.

TABLE III. Level density parameters for the statistical model calculations (Refs. 29 and 30).

Residue	(a/A) (MeV^{-1})	Δ (MeV)
^{14}N	0.176	0.00
^{12}C	0.164	5.13
^{16}O	0.164	5.13
^{20}Ne	0.164	5.13
^{23}Na	0.176	2.67
^{23}Mg	0.176	2.46
^{22}Na	0.176	0.00

Since the transmission coefficients given by the optical model include the direct reaction contribution to the absorption from the elastic channel, the compound-elastic cross section needs to be corrected. To perform a more realistic calculation of the compound-elastic contribution, a limit on the angular momentum for the compound nucleus was introduced. The introduction of an angular momentum cutoff can simulate the dynamical limits of the fusion process. A limit on the angular momentum introduced in the calculations can exclude the contribution from peripheral collisions to the compound nucleus formation. Similarly, if the compound nucleus itself does not survive at values of $J>J_C$, compound nucleus cross sections must be dependent on this limit. In either case, the introduction of a limiting angular momentum reduces the cross section for the formation of the compound system.

Values for the limiting angular momentum were extracted from fusion reactions studies.[20,21] Two sets of J_C as a function of the bombarding energy were considered. The use of the parameters derived by Ortiz and collaborators[20] reduces the maximum contribution of the compound-elastic process to the total cross section to about 10% of the DWBA process at 180°. The second set, derived by DeYoung and collaborators,[21] makes the compound-elastic cross sections even smaller, due to a smaller critical angular momentum derived in their work. With the introduction of the parameter J_C in the calculations, the total computed fusion cross section at 46 MeV is reduced by 26%, relative to the result obtained with no restriction on the angular momentum, and better agreement with the experimental fusion cross section is obtained. While cross sections for light-particle evaporation are slightly affected, the heavy residue channels suffer a reduction of as much as 70%.

Of equal importance to the statistical model calculations are the level density parameters. In the present calculation the value for the level density for the compound

nucleus was varied over a range of ±10%, but no significant changes in the cross sections were noticed. As a final consideration to the compound-elastic cross sections, an enhancement factor[22] for the elastic channel should be included. The inclusion of such a factor (of 2) gives a more realistic value for the compound-elastic contribution. In the present case, however, the results show that the maximum contribution from this channel with the enhancement factor taken into account is 20% of the elastic-transfer process at $\theta=176°$ and accounts for only 3% of the experimental cross section at this angle.

IV. DISCUSSION AND CONCLUSIONS

The contributions to the backward angle cross sections from the several different processes as evaluated for $E_{lab}=46$ MeV are shown in Fig. 3. Curves labeled (2) and (3) correspond, respectively, to the incoherent and coherent sums as defined by Eq. (1). The curve labeled (4) corresponds to the transfer of an α particle from an $L=4$ orbital to an $L=2$ orbital. The contribution from the compound elastic process without considering the enhancement factor is represented by curve (5). The solid line in this figure is the result of the addition of all these processes. Curve (1) shows how the angular distribution is modified when α transfer between $L=4$ orbitals only is taken into consideration together with elastic scattering process. The inclusion of the process in which an α particle is transferred from an $L=4$ to an $L=2$ orbital does not introduce significant changes in the angular distribution, although its contribution is stronger than that of the compound elastic channel.

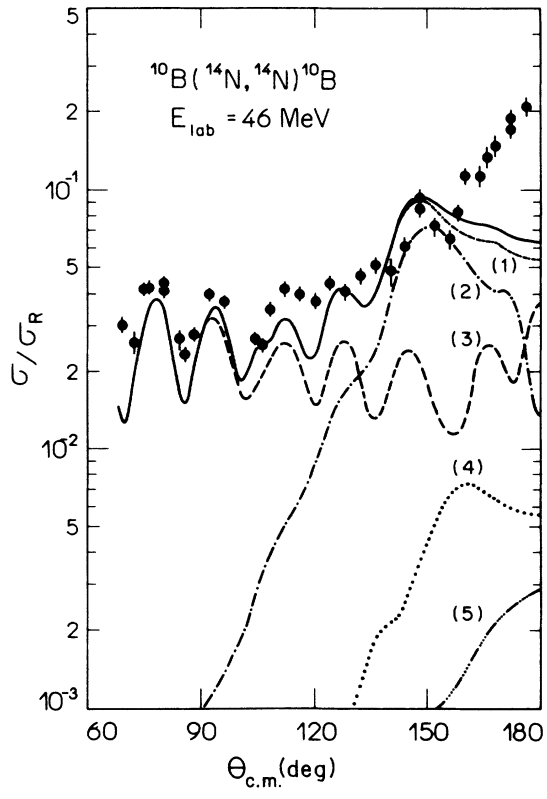

FIG. 3. A detailed comparison of the contributions for the backward angle elastic scattering as calculated in this work. The dashed line [curve(3)] represents the coherent sum between the elastic scattering amplitude and the $l=0$ alpha transfer. The incoherent sum for the alpha transfer with $l>0$ is shown by curve (2). The addition of these two processes result in curve (1). Curves (4) and (5) represent the elastic-transfer process between $L=4$ and $L=2$ orbitals and the contribution of the compound-elastic process, respectively. The solid line shows the addition of all contributions.

As shown here the α cluster exchange between projectile and target is quite large for the $^{10}B+^{14}N$ system. Over a large angular interval it explains quite satisfactorily the enhancement of the elastic cross section at backward angles. In the absence of data for angles beyond $\theta_{c.m.}=160°$ we would be lead to the conclusion that this is the only process responsible for this effect. Both shape and intensities are quite well reproduced with a spectroscopic factor of $S_4=0.65$, a value which is very close to the theoretical one derived by Kurath[9] ($S_4=0.69$) and to that measured by Wosniak and collaborators[7] ($S_4=0.41$) in the reaction $^{14}N(\alpha,^{8}Be)^{10}B$.

Enhancement of the cross section at back angles has also been observed[23] for a system ($^{9}Be+^{13}C$) similar to the one studied in the present work. Both systems are not made out of $n\alpha$ nuclei, and the colliding partners differ by an alpha particle. The data of Jarczyk *et al.*[23] have also been interpreted as due to an alpha cluster exchange between target and projectile and the elastic-transfer process describes the data satisfactorily. Their measurements, however, extend only to $\theta_{c.m.}=160°$. The results obtained in the present work give additional evidence for the importance of α-particle exchange in elastic collisions between nuclei in the $1p$ shell, even in the absence of an $n\alpha$ structure of the interacting nuclei.

The enhancement of the cross section at angles larger than 160° in the $^{14}N+^{10}B$ system still remains to be understood. In order to improve the evaluation of the elastic-transfer amplitude, higher order processes could be included. Possibly, a treatment based on multiple exchange of an α particle between target and projectile would be more general, although the exact mathematical treatment is rather difficult due to the nonzero spins of the nuclei. A possible way to guide this study would be on the basis of more phenomenological models.[24] Other transfer processes such as two-step deuteron transfer, with a $^{12}C+^{12}C$ intermediate state, could be present. Both deuteron transfer to ^{10}B and deuteron pickup from ^{14}N nuclei have been observed.[25] Experimental measurements of the $^{12}C+^{12}C$, $^{12}C^*+^{12}C$, and $^{12}C^*+^{12}C^*$ channels populated in the collision of ^{10}B and ^{14}N show high cross sections.[11] As the excitation function for the elastic scattering has been measured at 172°, a close study of it might reveal different reaction mechanisms involved. From the experimental point of view, the study of neighboring systems such as $^{14}N+^{11}B$ and $^{15}N+^{11}B$ certainly should bring additional valuable information for the understanding of the reaction processes involved.

ACKNOWLEDGMENTS

The authors would like to express their appreciation to E. M. Takagui, S. S. Vasconcelos, J. G. Pacheco, and M. S. Monsueto for their assistance in taking the data. Helpful discussions with N. Marquardt are gratefully acknowledged. This work was supported in part by Conselho Nacional de Desenvolvimento Cientifico e Tecnologico (CNPq) by Financiadora de Estudos e Projetos (FINEP) and by Fundacao de Amparo a Pesquisa do Estado de Sao Paulo (FAPESP).

---

*Present address: Physics Department, Brookhaven National Laboratory, Upton, NY 11973.

[1]P. Braun-Munzinger, G. M. Berkowitz, T. M. Cormier, J. W. Harris, C. W. Jachinski, J. Barrete, and M. J. Levine, Phys. Rev. Lett. **38**, 944 (1977).

[2]G. K. Gelbke, R. Bock, P. Braun-Munzinger, D. Fick, K. D. Hildebrand, W. Weiss, S. Wenneis, and G. Baur, Phys. Lett. **43B**, 284 (1973).

[3]R. M. DeVries, Nucl. Phys. **A212**, 207 (1973).

[4]C. F. MacGuire *et al.*, Phys. Rev. Lett. **53B**, 548 (1984).

[5]J. M. Mateja, A. D. Frawley, P. B. Nagel, and L. A. Parks, Phys. Rev. C **20**, 176 (1979).

[6]K. Koide, H. Takai, A. Bairrio Nuevo, Jr., and O. Dietzsch (unpublished).

[7]G. J. Wosniak *et al.*, Phys. Rev. C **14**, 815 (1976).

[8]T. Motobayashi, I. Kohno, T. Ooi, and S. Nakajima, Nucl. Phys. **A331**, 193 (1979).

[9]D. Kurath, Phys. Rev. C **14**, 815 (1976).

[10]N. Marquardt, private communication.

[11]W. Hoppe, Ph.D. thesis, Ruhr-Universität, 1984.

[12]T. M. Cormier and B. R. Fulton, Phys. Rev. C **22**, 565 (1980).

[13]K. Koide, A. Bairrio Nuevo, Jr., H. Takai, B. Marechal, and O. Dietzsch, Nucl. Instrum. Methods **215**, 177 (1983).

[14]H. Takai, K. Koide, A. Bairro Nuevo, Jr., E. M. Takagui, and O. Dietzsch (unpublished).

[15]W. Noremberg and H. Weidenmuller, *Introduction to Heavy Ion Collisions* (Springer-Verlag, Berlin, 1976).

[16]I. Talmi, Helv. Phys. Acta **25**, 185 (1952).

[17]R. M. DeVries, Phys. Rev. C **8**, 951 (1973).

[18]T. Tamura and K. S. Low, Comput. Phys. Commun. **8**, 349 (1974).

[19]R. G. Stokstad (unpublished).

[20]M. E. Ortiz *et al.*, Phys. Rev. C **28**, 692 (1980).

[21]P. A. DeYoung, J. J. Kolata, L. J. Satkowiak, and M. A. Xapsos, Phys. Rev. C **28**, 692 (1980).

[22]J. W. Tepel, H. M. Hofmann, and H. A. Weidenmuller, Phys. Lett. **49B**, 1 (1974).

[23]L. Jarczyk *et al.*, Nucl. Phys. **A316**, 139 (1977).

[24]W. E. Frahn *et al.*, Ann. Phys. (N.Y.) **101**, 166 (1981).

[25]G. Ishenko, H. Voit, E. Blatt, H. D. Helb, and E. Krwbsik, Nucl. Phys. **A123**, 497 (1969).

[26]A. Gobbi, R. Wieland, L. Chua, D. Shapira, and D. A. Bromley, Phys. Rev. C 7, 30 (1973).

[27]D. Shapira, R. G. Stokstad, and D. A. Bromley, Phys. Rev. C **10**, 1063 (1974).

[28]L. Zybert, R. Zybert, P. J. Nolan, and J. F. Sharpey-Schafer, Phys. Rev. C **24**, 111 (1981).

[29]U. Facchini and E. Saetta-Menichella, Energ. Nucl. (Paris) **15**, 54 (1968).

[30]A. Gilbert, A. G. W. Cameron, and F. S. Chen, Can. J. Phys. **43**, 1248 (1965).